nature metabolism

Supplementary information

https://doi.org/10.1038/s42255-026-01614-9

Gut microbiome maturation in early childhood interacts with host genetics to predict type 1 diabetes risk

In the format provided by the authors and unedited

Supplementary Figures

Supplementary Figure 1: Per-participant distribution of metagenomic stool samples across age.

Supplementary Figure 2: Association between host genetics and gut microbiome structure across developmental time points.

Supplementary Figure 3: Determination of the optimal number of microbiome maturational patterns. Diagnostic metrics for identifying the optimal number of clusters (k) using the traj package.

Supplementary Figure 4: Trajectory features representing 'measures of change' identified and selected for clustering by the trajectory clustering algorithm in the analysis of microbiome maturational patterns.

Supplementary Figure 5: Sensitivity analyses of microbiome maturation trajectories using alternative cluster numbers.

Supplementary Figure 6: Gut microbiome maturation patterns in the DIABIMMUNE cohort.

Supplementary Figure 7: Differential development of microbial processes involved in BCAA, AAA, galactose and vitamin B metabolism contributes to functional variation across microbiome maturational patterns.

Supplementary Figure 8: Time-stratified comparisons of Shannon diversity across maturation clusters.

Supplementary Figure 9: The distributions of SNP loadings for the top five genetic PCs are shown for all chromosomes.

Supplementary Figure 10: PC2 and PC3 capture distinct and orthogonal genetic signals.

Supplementary Figure 11: Gene set enrichment analysis based on SNP loadings from the third principal component of the host genetic PCA.

Supplementary Figure 12: The impact of population genetic structure on baseline composition and temporal changes in the gut microbiomes of infants (0-540 days) and toddlers (541-1,095 days).

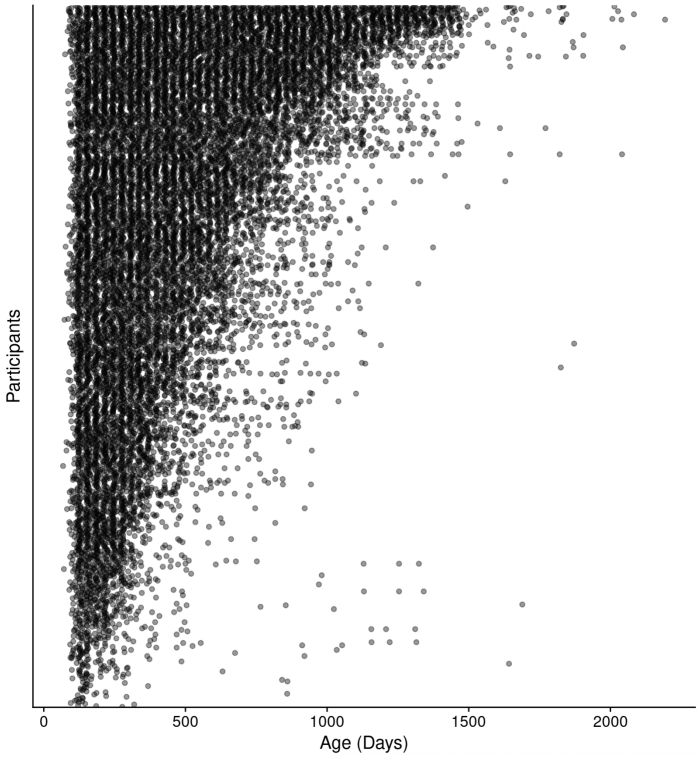

Supplementary Figure 1. Per-participant distribution of metagenomic stool samples across age. Stool samples were collected approximately monthly through 48 months of age and quarterly thereafter, per the TEDDY protocol. Because TEDDY is a dynamic prospective cohort study with right-censored follow-up at the analytic cutoff, per-participant follow-up duration is variable. A subset of these samples was selected for shotgun metagenomic sequencing, yielding 12,151 metagenomes across 887 participants (mean 13.7 ± 8.7 sequenced samples per participant over the during follow-up). Each dot represents one shotgun-sequenced stool sample from the analyzed dataset. The y-axis represents individual participants, sorted by sample density; the x-axis represents participant age in days at the time of sample collection. The plot illustrates the longitudinal sampling structure of the cohort, including inter-individual variability in follow-up duration and sampling density. Consistent with the TEDDY protocol and with prior TEDDY microbiome studies (Stewart et al., 2018; Vatanen et al., 2018), sampling is densest during early life (approximately 0-1,400 days, corresponding to the first ~4 years) and becomes sparser thereafter.

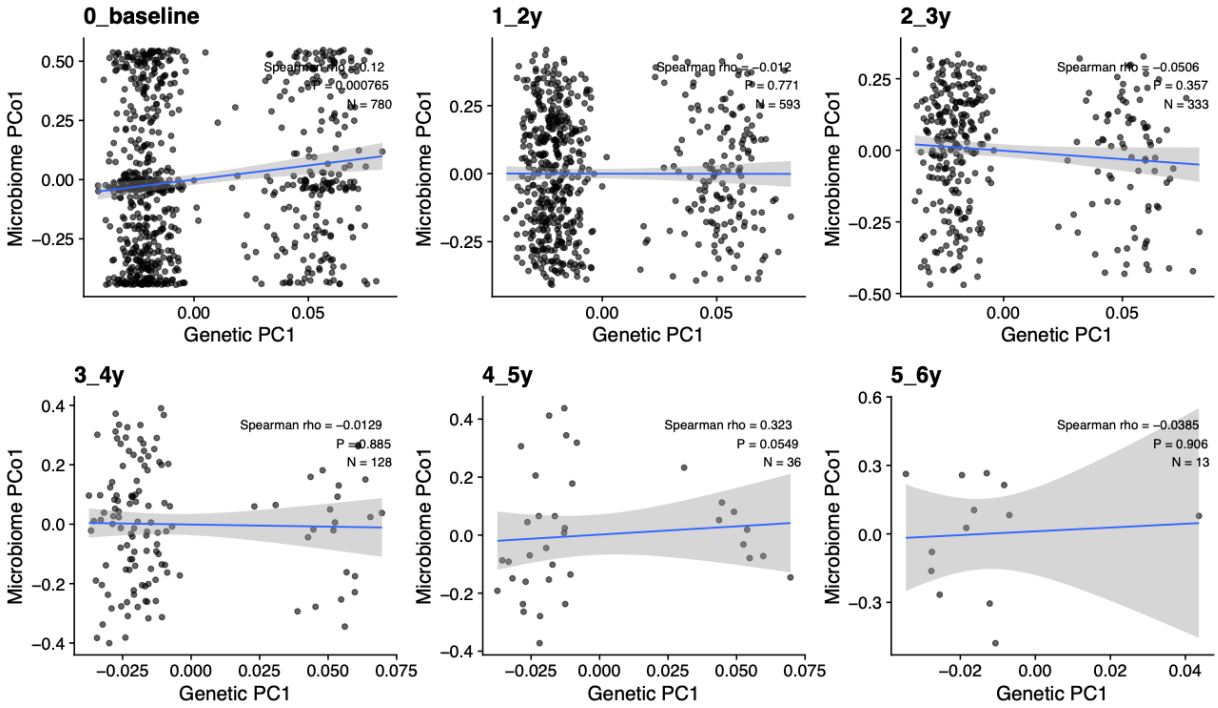

Supplementary Figure 2. Association between host genetics and gut microbiome structure across developmental time points. Each panel shows the association between genetic PC1 and microbiome PCo1 at a given developmental time point. To ensure sample independence, a single sample per participant was included at each time point, defined as the earliest available sample within the corresponding time window. Points represent individual subjects. Blue lines indicate fitted linear regression lines and gray shading indicates 95% confidence intervals. Corresponding correlation coefficients, P values, and sample sizes are shown in each panel.

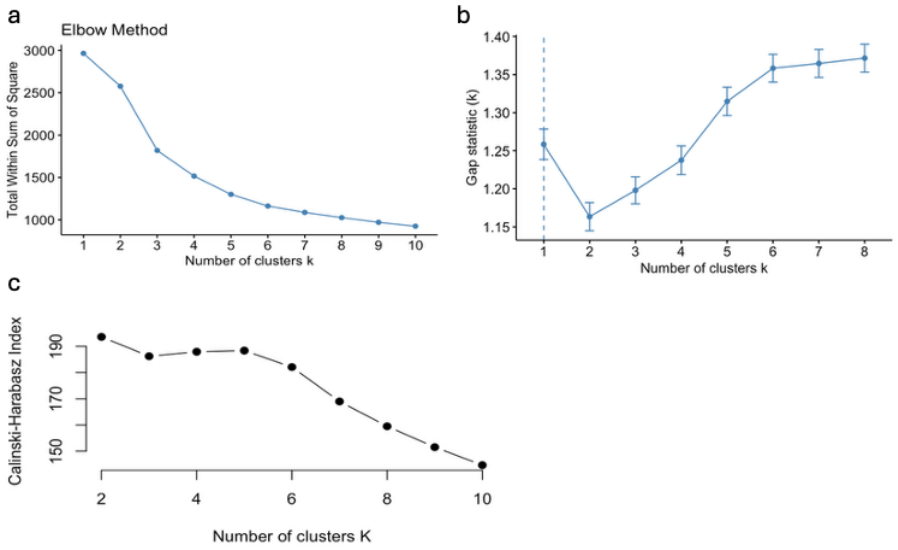

Supplementary Figure 3: Determination of the optimal number of microbiome maturational patterns. Diagnostic metrics for identifying the optimal number of clusters (k) using the traj package. (a) The Elbow Method showing the Total Within Sum of Squares; a distinct inflection point is observed at k=3. (b) The Gap Statistic (mean±SE). (c) The Calinski-Harabasz Index; the score remains high at k=3 before declining, indicating good cluster separation. The final selection of k=3 balances the inflection in the Elbow method and the high CH index with the need for an adequate sample size per cluster for downstream statistical inference.

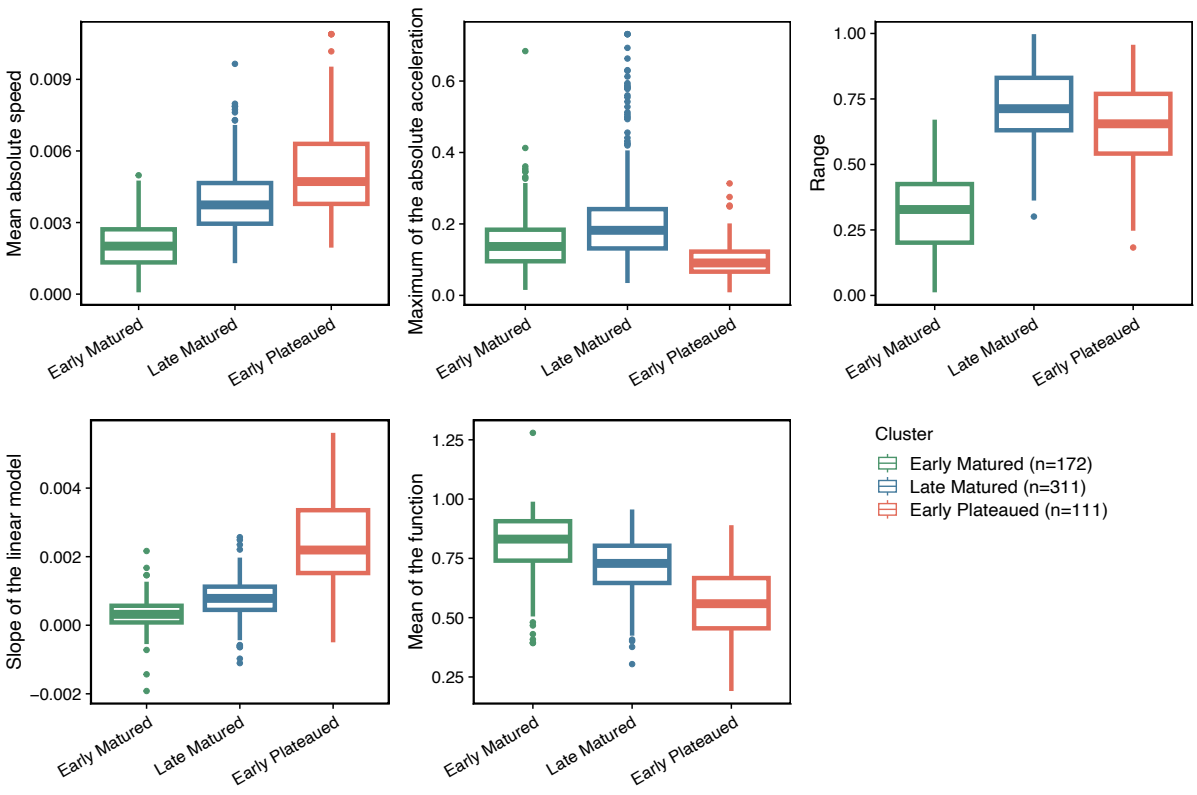

Supplementary Figure 4. Trajectory features representing 'measures of change' identified and selected for clustering by the trajectory clustering algorithm in the analysis of microbiome maturational patterns. The five most informative features were chosen for k-means clustering through the following process: Features that remained constant across trajectories were excluded due to their lack of discriminative power. Principal Component Analysis (PCA) was then performed, and the principal components contributing more to the total variance than any single measure were identified. A varimax rotation was applied to these components, after which the measure most strongly correlated with each rotated component was selected, beginning with the component that explained the greatest variance. Box plot centers show medians of each measure with boxes indicating their inter-quartile ranges (IQRs), and upper and lower whiskers indicating 1.5 times the IQR from above the upper quartile and below the lower quartile, respectively.

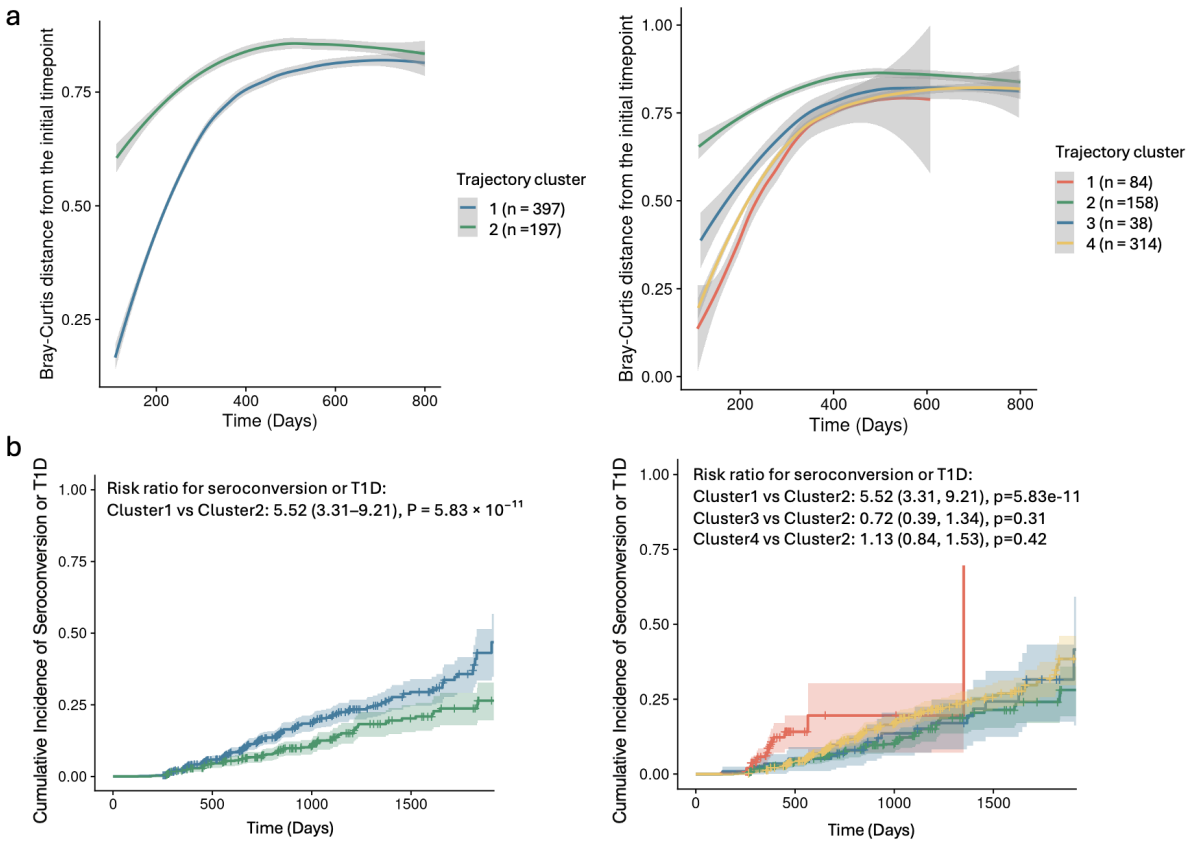

Supplementary Figure 5. Sensitivity analyses of microbiome maturation trajectories using alternative cluster numbers. (a) Sensitivity analyses using alternative numbers of trajectory clusters. Left, trajectory clustering with k = 2 identified two broad microbiome maturation patterns. Right, trajectory clustering with k = 4 identified four maturation patterns. Clusters were derived using a trajectory clustering algorithm based on Bray–Curtis distances from each participant's baseline gut microbiome composition across visits during the first 800 days of life. Trajectories were smoothed and visualized using LOESS curves; shaded bands indicate 95% confidence intervals. (b) Association between alternative maturation patterns and risk of islet autoantibody seroconversion or type 1 diabetes (T1D). Left, cumulative incidence curves and hazard ratio estimates for the two-cluster solution. Right, cumulative incidence curves and hazard ratio estimates for the four-cluster solution. Hazard ratios were estimated using multivariable Cox proportional hazards models adjusting for clinical center, sex, antibiotic use, probiotic use, breastfeeding cessation, age at solid food introduction, and the top five host genetic principal components. Shaded bands indicate 95% confidence intervals. Consistent results across clustering resolutions indicate that the association between impaired/non-progressive microbiome maturation and T1D risk is robust to the choice of k.

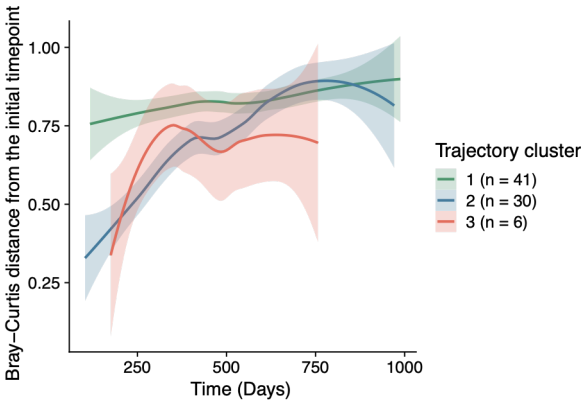

Supplementary Figure 6. Gut microbiome maturation patterns in the DIABIMMUNE cohort. (a) Using the same trajectory clustering framework applied in TEDDY, we identified three data-driven gut microbiome maturation patterns in early life. The patterns were identified using a trajectory clustering algorithm that employs the Bray-Curtis distance to quantify changes in the gut microbial composition from baseline across subsequent visits during the initial 1000-day period.

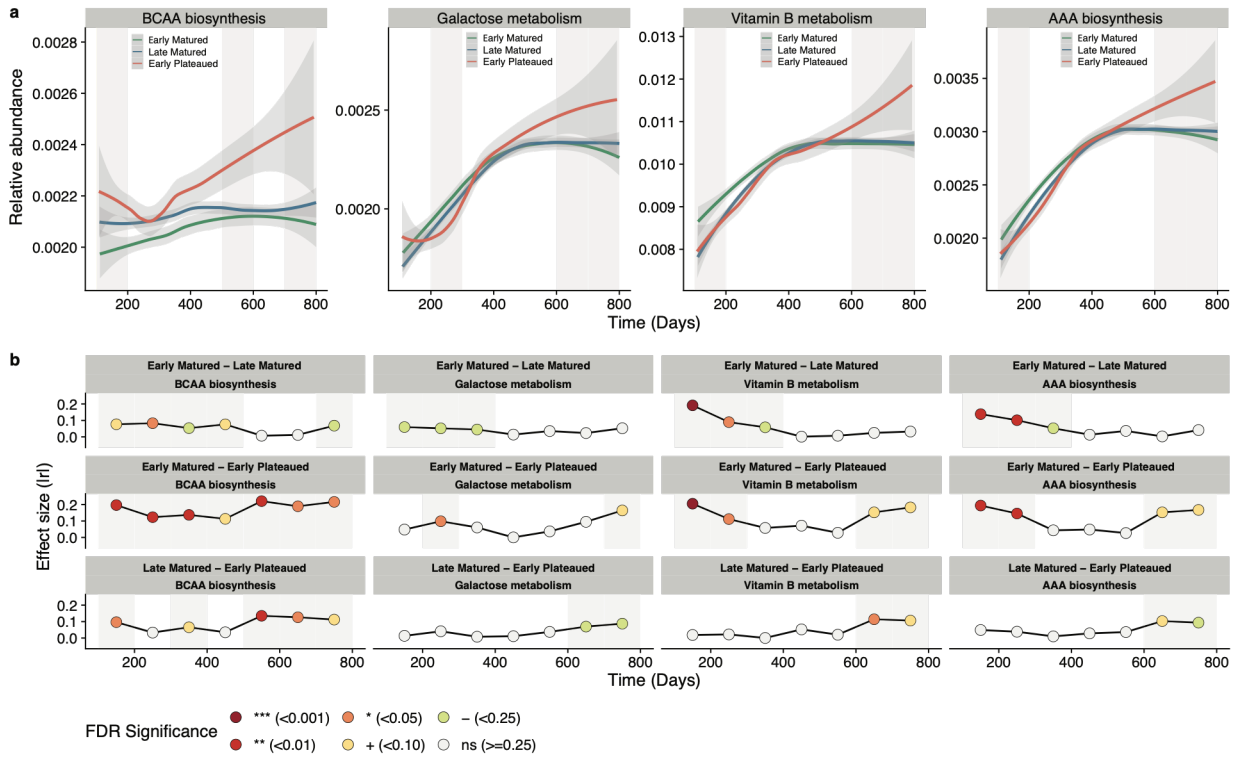

Supplementary Figure 7: Differential development of microbial processes involved in BCAA, AAA, galactose and vitamin B metabolism contributes to functional variation across microbiome maturational patterns. (A) Temporal trajectories of microbial enzyme abundances involved in aromatic amino acid (AAA) biosynthesis, branched-chain amino acid (BCAA) biosynthesis, galactose metabolism, and vitamin B/co-factor metabolism across the three microbiome maturational patterns (Early Matured, n=172; Late Matured, n=311; Early Plateaued, n=111). Lines represent LOESS-smoothed fitted values, and shaded areas indicate 95% confidence intervals. Shaded background indicates the top three 100-day bins showing the strongest between-cluster differences, based on Wilcoxon rank-sum tests. (B) Rank-biserial effect sizes (r) for pairwise comparisons between clusters within each 100-day bin, calculated using the Wilcoxon rank-sum test. Points are colored according to significance after Benjamini–Hochberg (BH) FDR correction. All bins with significant differences (FDR < 0.25) are shaded.

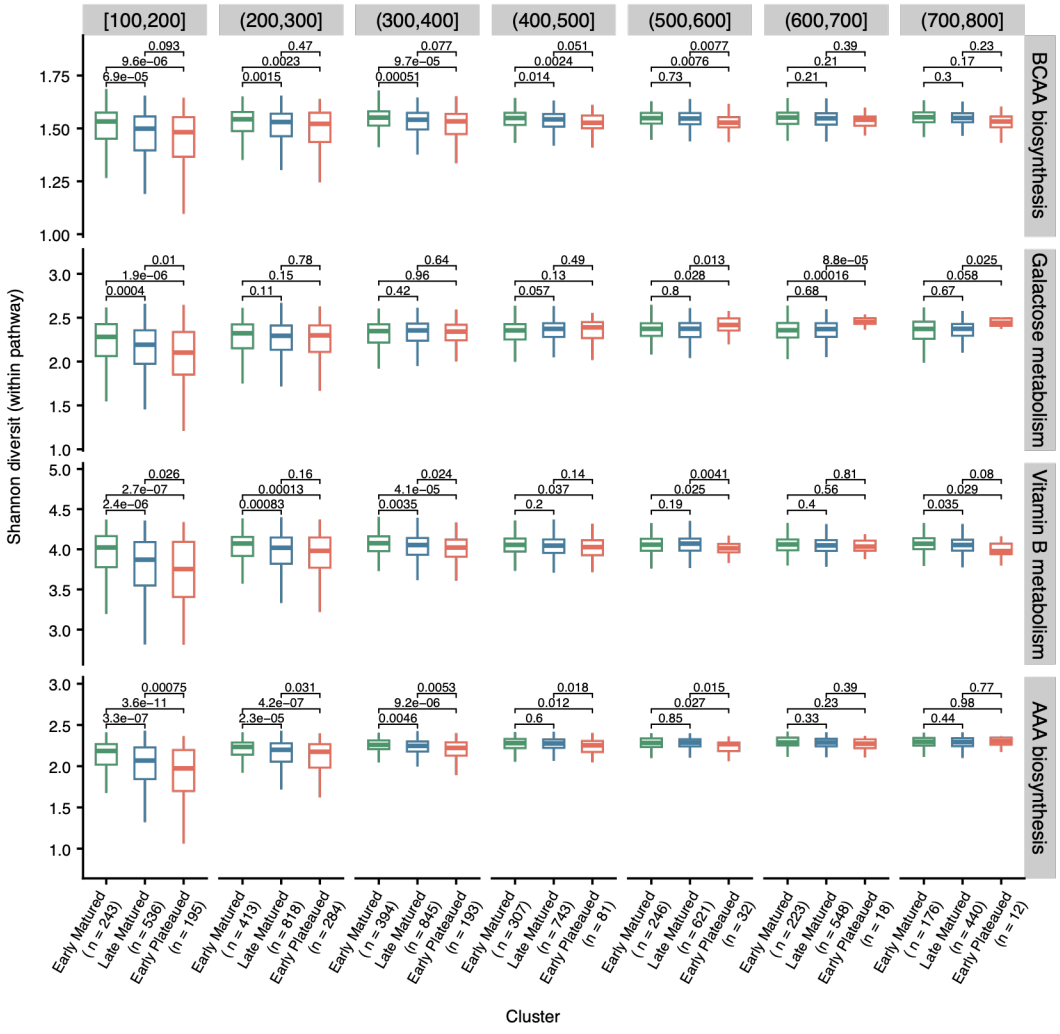

Supplementary Figure 8. Time-stratified comparisons of Shannon diversity across maturation clusters. Pathway-level Shannon diversity of EC composition is shown across microbiome maturation clusters over time. Boxplots show pathway-level Shannon diversity of EC composition across microbiome maturation clusters within each time bin. The center lines represent the medians of the Shannon Diversity Index. The boxes show the interquartile ranges (IQRs; 25th–75th percentiles), and whiskers extend to the most extreme values within 1.5 times the IQR from the lower and upper quartiles, respectively. Two-sided Wilcoxon rank-sum tests were used for pairwise comparisons within time bins. The n indicates the number of longitudinal stool samples in each group.

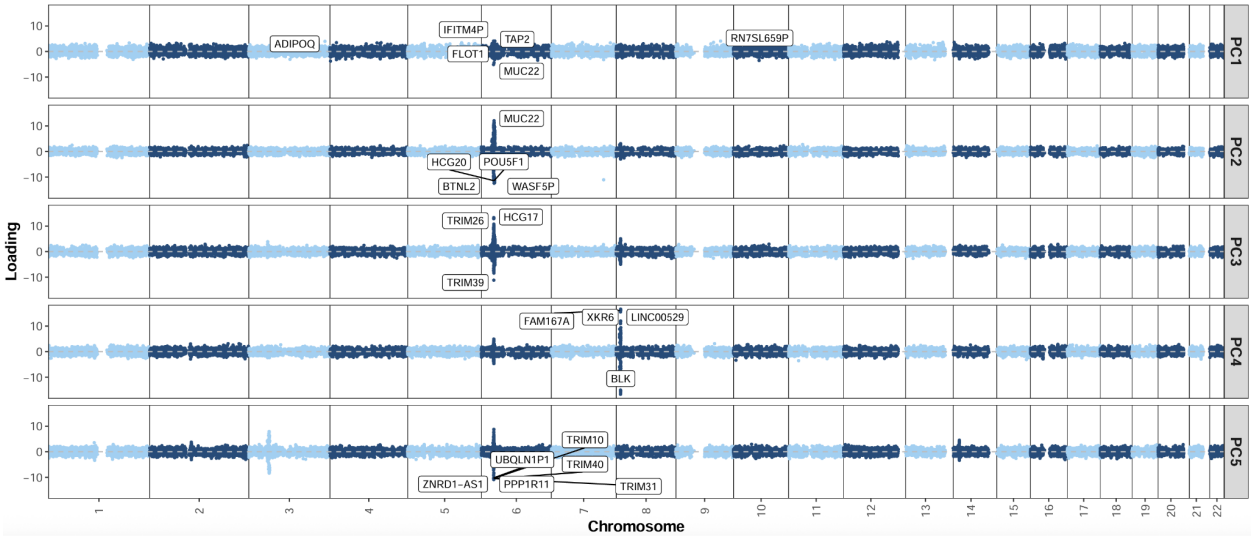

Supplementary Figure 9: The distributions of SNP loadings for the top five genetic PCs are shown for all chromosomes. SNPs with high loadings in PC2 and PC3 are concentrated within the major histocompatibility complex. The top absolute loading SNPs in each PC were annotated using the nearest gene within 5 kb.

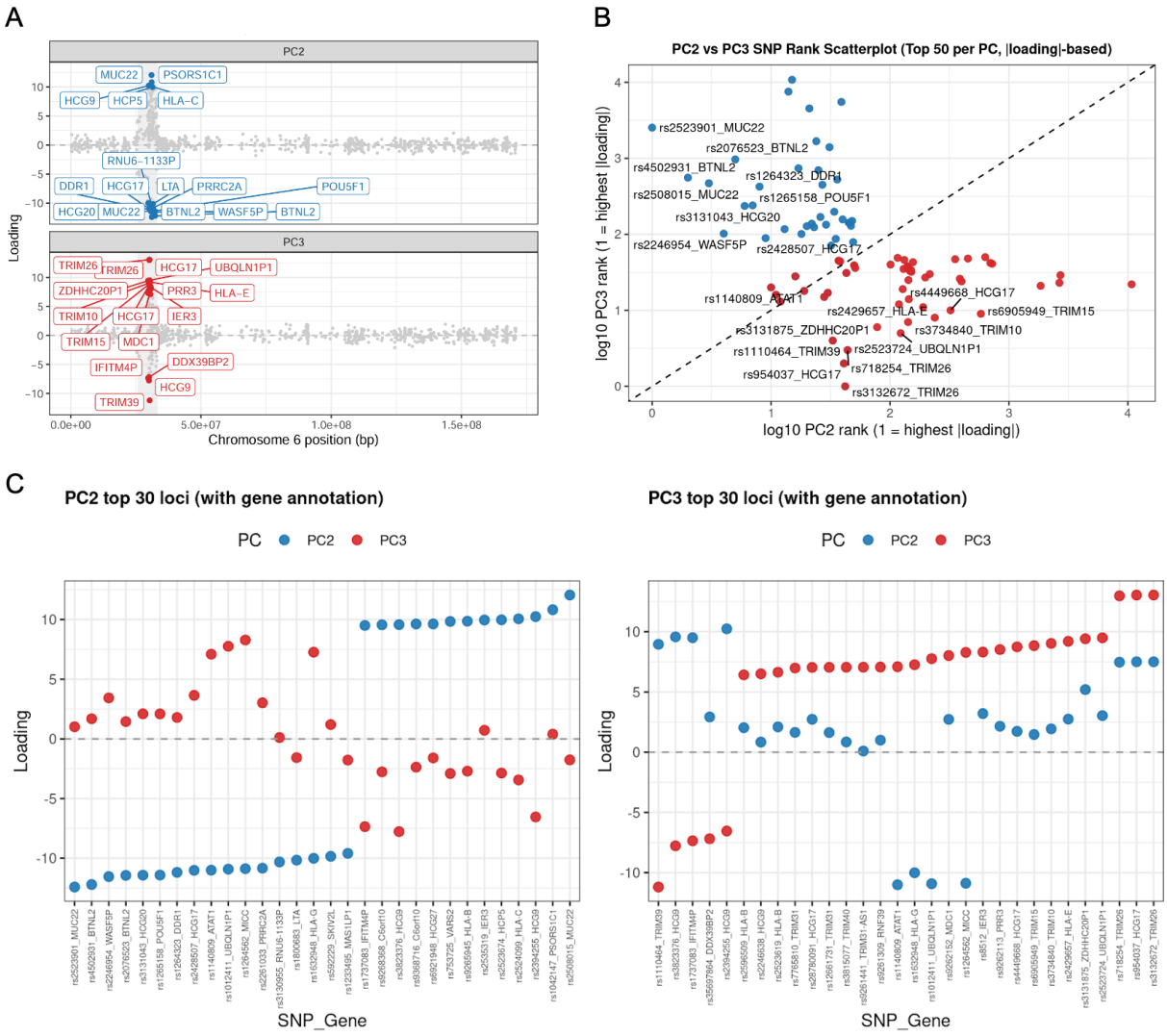

Supplementary Figure 10. PC2 and PC3 capture distinct and orthogonal genetic signals. (A) The Manhattan plots display the distribution of SNP loadings along chromosome 6 for PC2 (top panel) and PC3 (bottom panel). SNPs with the highest absolute loadings for each component are highlighted and annotated using the nearest gene within 5 kb of the variant. (B)The scatterplot displays the top SNPs for PC2 and PC3 (top 50 SNPs per PC, ranked by absolute loading). Each point represents a SNP, plotted according to its log10 rank in PC2 (x-axis) and PC3 (y-axis). Blue points indicate SNPs ranked within the top loadings for PC2, and red points indicate those ranked within the top loadings for PC3. The diagonal dashed line marks equal rank between the two components. (C) The two-panel scatterplot displays the top 30 SNPs for PC2 (left) and PC3 (right), ranked by absolute loading, with gene annotations shown along the x-axis. Each point represents the loading of the same SNP on PC2 (blue) and PC3 (red), enabling direct comparison of their contributions to each component. Blue points indicate the SNP's loading on PC2, whereas red points indicate its loading on PC3. The dashed horizontal line denotes zero loading.

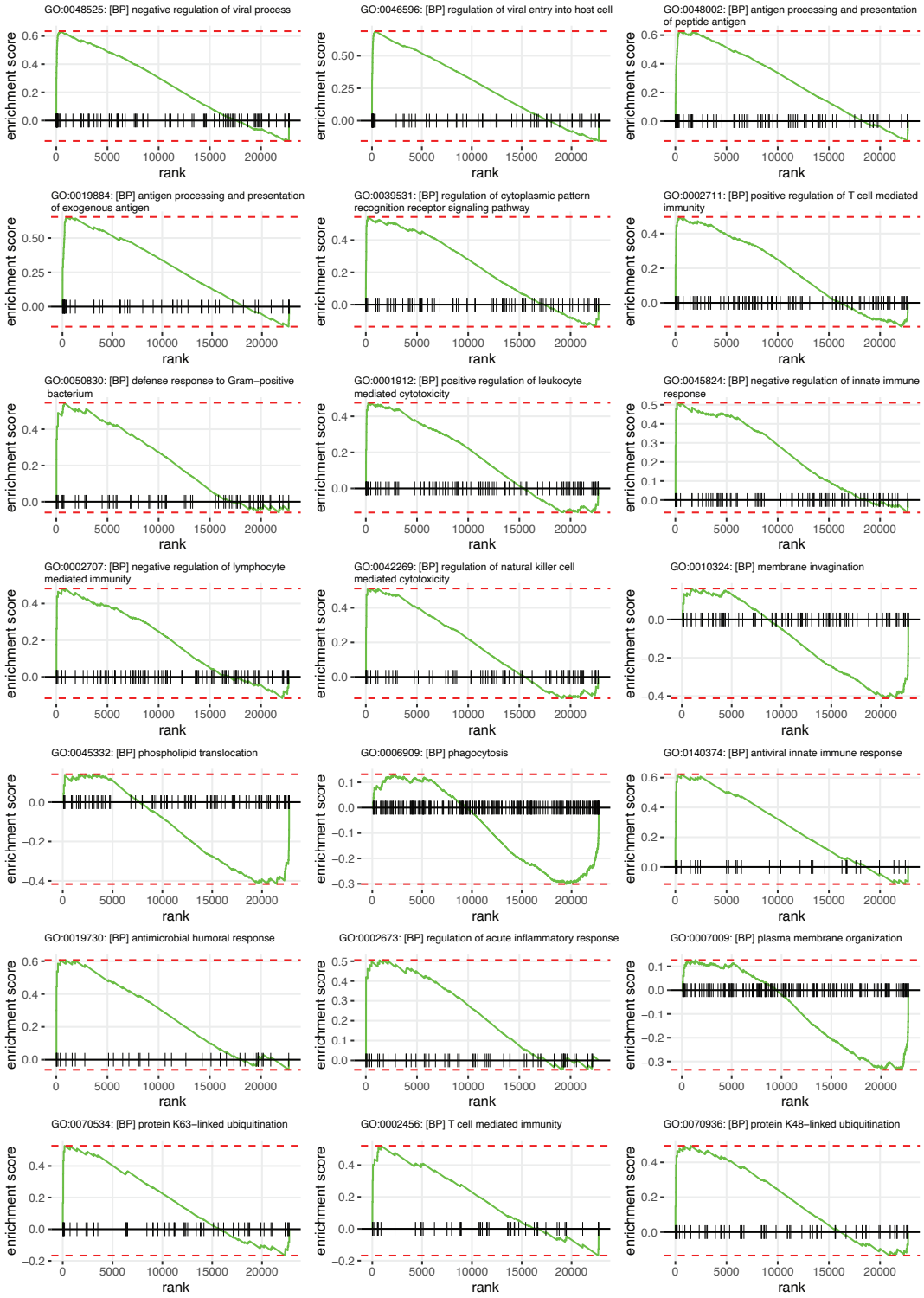

Supplementary Figure 11. Gene set enrichment analysis based on SNP loadings from the third principal component of the host genetic PCA. The line plots show the running enrichment scores for the gene ontology (GO) terms for biological processes as the analysis 'walks down' the ranked list. The vertical black lines on the X-axis indicate where members of the GO terms (at the SNP level) appear in the ranked list of all QCed SNPs in Immunochips (linkage disequilibrium < 0.2).

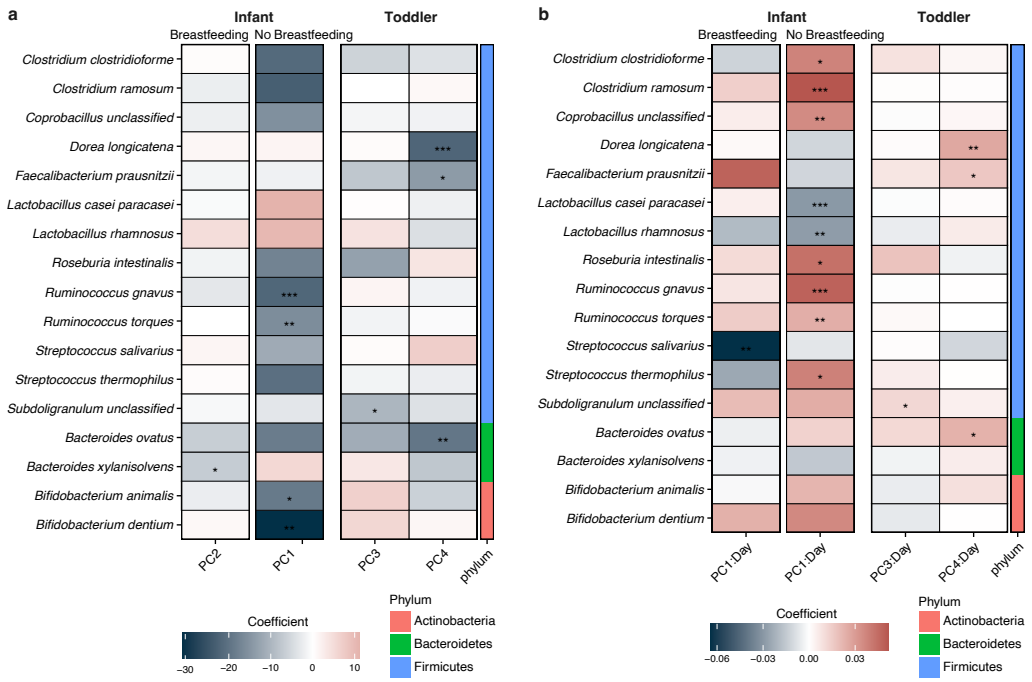

Supplementary Figure 12: The impact of population genetic structure on baseline composition and temporal changes in the gut microbiomes of infants (0-540 days) and toddlers (541-1,095 days). (A) The population genetic structure, summarized by genetic principal component (PC) scores, was associated with diverse microbial species at baseline (quantified by the beta coefficients of the PCs). (B)The population genetic structure, summarized by genetic principal component (PC) scores, was associated with diverse microbial species developmental trajectories (quantified by the beta coefficients of the interaction terms between a PC and time). The associations in both panels were quantified using linear mixed models that include participants' IDs as random effects and clinical center, genetic PCs, time, and interaction terms between a genetic PC and time as fixed effects. The color gradient from blue to red represents the effect size of these associations, with the significance level (Bonferroni-adjusted P-values) indicated. * Adjusted $P < 0.05$, ** Adjusted $P < 0.01$, *** Adjusted $P < 0.001$.